Journal of Environmental Chemical Engineering 13 (2025) 115128

Contents lists available at ScienceDirect

Journal of Environmental Chemical Engineering

journal homepage: www.elsevier.com/locate/jece

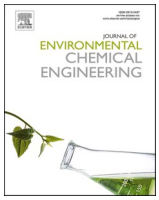

Selective biphasic oxidation of nitrogenated contaminants with H_2O_2 using polyolefin-derived carbon nanotubes

Fernanda F. Roman [a,b,c,*], Larissa de G. Piccinin [a,d], Adriano S. Silva [a,b,c], Jose L. Diaz de Tuesta [e], Admilson Vieira [d], Adrián M.T. Silva [b,c], Joaquim L. Faria [b,c], Helder T. Gomes [a,*]

[a] CIMO, LA SusTEC, Instituto Politécnico de Bragança, Campus de Santa Apolónia, Bragança 5300-253, Portugal
[b] LSRE-LCM – Laboratory of Separation and Reaction Engineering - Laboratory of Catalysis and Materials, Faculty of Engineering, University of Porto, Rua Dr. Roberto Frias, Porto 4200-465, Portugal
[c] ALiCE – Associate Laboratory in Chemical Engineering, Faculty of Engineering, University of Porto, Rua Dr. Roberto Frias, Porto 4200-465, Portugal
[d] Universidade Tecnológica Federal do Paraná, Campus Londrina, Londrina 86036-370, Brazil
[e] Chemical and Environmental Engineering Group, ESCET, Rey Juan Carlos University, Tulipán s/n, Móstoles 28933, Spain

ARTICLE INFO

Keywords:
Fuel denitrogenation
Nanostructured carbon
Valorization of wastes
Circular economy
Plastics recycling

ABSTRACT

Liquid/liquid biphasic oxidations are extensively employed in the chemical industry to manufacture a variety of chemicals and for environmental issues, such as the oxidative denitrogenated (ODN) and desulfurization of fuels. The ubiquitous presence of nitrogenated and sulfonated compounds in petroleum-derived fuels is associated with environmental and health issues, driving legislation to become stricter regarding the content or related emissions of those impurities. However, catalysts with high performance, low cost and high activity towards selective oxidation of targeted contaminants should be developed. This work deals with the oxidative denitrogenation of quinoline and pyridine, used as model nitrogenated compounds, using carbon nanotubes as catalysts, which were derived from polyolefins (low-density polyethylene, high-density polyethylene and propylene) representative of plastic solid waste (PSWs) mixtures found in municipal solid wastes. The carbon precursor used offers not only a solution to reduce PSWs accumulation in waste management systems but also a cheap feedstock for preparing CNTs. All PSWs-derived CNTs allowed to remove quinoline completely, pyridine, and both of them in a mixture under the same conditions (1 h, 80 °C, c_{cat} = 2.5 g L^{-1}, $[H_2O_2]_0$ = 247 g L^{-1}, O/W volume ratio = 80:20, $[N]_0$ = 108 mg L^{-1}). These results were maintained for up to 5 additional reuse cycles for the catalyst prepared with mixed polyolefins.

1. Introduction

Fuels are crucial for meeting energy demands, particularly in transportation [1]. Impurities, such as sulfur (<6 wt%), nitrogen (<2 wt%), oxygen (<1.5 wt%) and heavy metals, are usually present in crude oils, posing health [2,3] and environmental issues [4,5], and sulfur was even reported as an impurity for some renewable fuels [6] with a concentration up to 850 ppm [7]; and resulting in stricter legislation [8]. Removal of N and S compounds from liquid fuels is a key step in refineries, usually achieved through hydrotreatment processes conducted at high temperatures (260 – 425 °C) and H_2 partial pressures (5–170 bar) [8]. However, hydrotreatment may fail to achieve the legally allowed S or N content. Thus, alternative processes to complement HDS and HDN have been proposed [9–11], and oxidation-based treatments (oxidative desulfurization (ODS) and denitrogenation (ODN) for targeted *S* and *N* removals, respectively) are seen as promising processes [8], with milder operating conditions (25–140 °C and 1–2 bar) compared to HDS/HDN. The removal of organosulfur compounds by oxidation (ODS) has been much more studied than ODN in the past 20 years (Figure S1), mainly because organosulfur compounds are directly regulated and considered more harmful than *N*-compounds. Nevertheless, with the expected decrease of allowed NO_x emissions by the implementation of Euro VII [12], the effect of *N*-compounds over a series of fuel parameters [13] and the recalcitrant behavior of those compounds towards HDN, ODN emerges as an important alternative to target the removal of *N*-compounds from fuels. Other non-hydrogen processes are also available,

* Corresponding authors at: CIMO, LA SusTEC, Instituto Politécnico de Bragança, Campus de Santa Apolónia, Bragança 5300-253, Portugal.
E-mail addresses: roman@ipb.pt (F.F. Roman), htgomes@ipb.pt (H.T. Gomes).

https://doi.org/10.1016/j.jece.2024.115128
Received 1 August 2024; Received in revised form 2 December 2024; Accepted 14 December 2024
Available online 16 December 2024

such as adsorptive and extractive denitrogenation, however, they have limitations, such as longer hours of operation [14] or high volumes of solvents [15].

ODN can be classified as a selective oxidation process, as it can be conducted using a biphasic medium [8]. Hydrogen peroxide aqueous solutions are interesting oxidant sources, as they can act simultaneously as both oxidant and extraction phases for oxidized products. Hydrogen peroxide also offers advantages such as low cost, ease of use, and being environmentally friendly. The ODN process in biphasic systems also requires suitable catalysts to increase the oxidation reaction rate and facilitate mass transfer, acting as phase transfer catalysts [16,17]. Carbon-based materials, especially carbon nanostructured materials (CNMs) such as carbon nanotubes (CNTs), are interesting options, as they have been shown to catalyze oxidation reactions either in the liquid phase [18–21] and in biphasic media [22,23]. Furthermore, their hydrophilic-hydrophobic characteristics can be easily tuned [24] for better contact between oily and water phases. Previous studies have reported the use of carbon nanotubes for the selective removal of nitrogenated compounds using H_2O_2 as an oxidant source. For instance, Janus-structured CNTs obtained from C_2H_4/CH_3CN have been reported for the selective removal of a range of N-containing materials under oil-water emulsified systems, including QN (30–100 % in 40 min [25] and 40–85 % in 45 min [26]), 4-nitrophenol (50–100 % in 4 h) [22], 2-nitrophenol (20–80 % in 24 h) [23]. Other CNTs have also been reported for selective oxidation of QN under emulsified oil-water systems, resulting in 80–100 % in 60 min [27,28] and 100 % in 30 min [29]. However, most of those studies focus on CNTs synthesized from non-renewable carbon sources typically derived from petroleum, such as pure ethylene or methane gases; and the use of waste sources for catalyst synthesis could render the process more sustainable.

Another global concern is the accumulation of mixed and contaminated plastic solid waste (PSWs) in waste management systems, posing a significant challenge for recycling facilities. According to the Eurostat database, plastic packaging waste reaches 35.92 kg per capita in 2021 (more recent data at the publication of this research paper), whereas 31.53 kg per capita was produced in 2016 [30]. Additionally, the recycling rate decreases from 42.4 % to 39.7 % in the same period [31]. Therefore, the development of recycling technologies is a priority for sustainable development. According to projections [32], conventional and innovative approaches will be required to effectively decrease the amount of microplastics reaching aquatic and terrestrial environments [32]. Polyolefins are largely found in the composition of contaminated PSWs, mainly because they are frequently used for packaging and thrown out after a single use [33]. Nonetheless, polyolefins are mainly made of carbon atoms (low-density polyethylene and high-density polyethylene, LDPE and HDPE, respectively, and polypropylene, PP, are made up of 85.6 % of carbon [34]), meaning that they can be transformed into carbon-based materials, including CNTs [18,35–38]. The synthesis of CNTs from plastic waste has been shown to benefit the environment, considering the negative effects of climate change, fossil fuel depletion, and toxicity due to the accumulation of this waste type in diverse ecosystems [39].

In this context, this work aims at improving the sustainability of the removal of N-compounds from fossil fuels, by studying effective catalysts derived from simulated waste sources for the selective oxidation of N-compounds, thus also proposing a solution to address the accumulation of PSW in waste management systems. With this focus, CNTs were prepared using a single-stage reactor, considering polyolefins (LDPE, HDPE and PP) as representative polymers of PSWs over iron nanoparticles. The obtained CNTs were then applied as catalysts in the abatement of quinoline (QN) under a biphasic system consisting of an oily phase (2,2,4-trimethylpentane) containing QN and an H_2O_2 aqueous phase (acting simultaneously as extractant and oxidant source). CNTs prepared with a mixture of polyolefins were further used to remove pyridine (PYR) and a multi-component system containing QN and PYR. Few papers in the literature deal with the ODN of QN under a green system combined with materials obtained from sustainable sources.

2. Materials and methods

2.1. Reagents and materials

Alumina (D10–10) was obtained from BASF as 4 mm pellets. It was initially ground and sieved to obtain particle sizes in the 53–106 μm range. High-density polyethylene (HDPE, melt index 2.2 g/10 min), low-density polyethylene (LDPE, weight average molecular weight ~35,000 g/mol, number average molecular weight ~7700), polypropylene (PP, weight average molecular weight ~250,000 g/mol, number average molecular weight ~67,000 g/mol), carbon nanotubes (HWCNT, multi-walled), and titanium(IV) oxysulfate (~15 wt% in diluted sulfuric acid, 99.99 % trace metal basis) were supplied by Sigma-Aldrich. Ethanol absolute (99.8 %), ethylene glycol (99 %), acetonitrile (99.9 %), and orthophosphoric acid (85 %) were obtained from Fisher Chemical. Quinoline (98 %) and sulfuric acid (98 %) were supplied by Alfa Aesar and Labkem, respectively. Iron(II) chloride tetrahydrate (98 %) was provided by Acros Organics. Iron(III) chloride hexahydrate (98 %), 2,2,4-trimethylpentane (99.9 %), hydrogen peroxide (30 %), sodium hydroxide (99.2 %), and pyridine (99.9 %) were provided by VWR Chemicals. Spray mount was obtained from 3 M. All reactants were used without modifications. Ultrapure water was used throughout the work.

2.2. Synthesis of carbon nanotubes

The CNTs were synthesized via chemical vapor deposition (CVD) over iron nanoparticles supported on alumina (Fe-NP/Al_2O_3) following a sol-gel methodology, as previously described [21,40]. The CVD process occurred in a single-stage vertical oven (TH/TV, Termolab), considering LDPE, HDPE and PP, either individually or in a mixture of the three polymers (MIX), as carbon sources. The mixture of three polymers considered a ratio of 35:25:40 of LDPE:HDPE:PP (in mass basis), these proportions between the distinct polyolefins being chosen according to real reports of PSW composition in municipal streams [33]. The configuration of the oven is shown elsewhere [20]. The CNTs were labeled according to the polymeric feedstock and temperature used in the CVD process: LDPE-600@Fe, LDPE-800@Fe, HDPE-800@Fe, PP-800@Fe and MIX-800@Fe. Only LDPE was tested at 600 °C as it has been reported that LDPE results in a higher amount of gaseous fractions (especially C1-C2 fraction) compared to HDPE and PP [41] in the thermal pyrolysis process, which should favor the formation of CNMs.

2.3. Materials characterization

X-ray diffraction (XRD) was acquired in a PANalyticalX'Pert PRO X-ray diffractometer equipped with a X'Celerator detector and secondary monochromator (Cu Kα $\lambda = 0.154$ nm). Data analysis and treatment were performed using X'Pert HighScore Plus software and the Crystallography Open Database (COD) for phase identification and semi-quantitative estimation of the components. TEM images were acquired in a JEOL 1011 transmission electron microscope operating at 200 kV. The hydrophobicity/hydrophilicity of the samples was estimated by static water contact angle measurements using the sessile-drop method. The measurements were performed in a glass slide covered by the materials with a spray adhesive from 3 M, prepared according to a procedure described elsewhere [42,43]. Image acquisition was carried out using a Attention optical tensiometer (model Theta), and data analysis was carried out in ImageJ. The contact angles reported are an average of at least 3 measurements in different locations of the slides. Basicity/acidity characterization was performed by adapting a procedure reported in another work [44]. Briefly, 50 mg of each CNT was added into either a

0.02 M HCl or 0.02 M NaOH solution for 24 h under stirring (400 rpm) at room temperature. After 24 h, the solids were separated from the liquid and titrated against the opposing solution. Thermogravimetric analysis (TGA) was conducted in a NETZSCH TG 209F3 equipment under a nitrogen atmosphere (40–890 °C, 10 °C min^{-1}). The remaining weights at the end of the TGA analysis were used to estimate the volatile content of the samples, and the remaining weights at T = 100 °C were used to estimate the moisture content of the samples. The ashes contents were determined using a muffle at 800 °C. The ashes recovered were then digested using *aqua regia* (HNO_3:HCl molar ratio of 1:3) at 105 °C for 12 h; the resulting liquid was analyzed via atomic absorption spectroscopy (PinAacle 900 T, Perkin Elmer, Hongkong, China) to determine the iron content in the ashes (Fe_{ashes}). The C, H and O content were obtained by elemental organic analysis using a Flash 2000 analyzer (Thermo Fisher Scientific,Waltham, MA, USA) provided with a thermal conductivity detector. Raman spectra were acquired in an Alpha 300 (WiTec, Germany) at a monochromatic wavelength of 532 nm. The magnetic response of the samples was qualitatively assessed with a neodymium magnet.

2.4. Reaction runs

2.4.1. Extraction and adsorption of QN

The pure extraction effect was estimated considering different initial concentrations of QN in 2,2,4-trimethylpentane ($[QN]_0^{oil}$ = 250 – 1000 mg L^{-1}, equivalent to $[N]_0^{oil}$ = 27 – 108 mg L^{-1}). The QN solution was placed in a reaction vessel and heated to 80 °C. Upon reaching the desired temperature, a volume of ultrapure water at pH 3.0 (adjusted using H_2SO_4 0.5 M, not buffered) already at 80 °C was added, considering this t_0 = 0 min. The ratio between 2,2,4-trimethylpentane and water was kept at O/W = 80:20 v/v, and the medium was well stirred (600 rpm). The concentration of QN in both oil and water phases ($[QN]^{oil}$ and $[QN]^{water}$, respectively) was followed by UV-Vis. The samples were withdrawn in such a way as to ensure that the O/W ratio was not changed.

The adsorption effect in the oil phase was also evaluated by placing a QN solution ($[QN]_0^{oil}$= 1000 mg L^{-1}, $[N]_0^{oil}$ = 108 mg L^{-1}) in a reaction vessel and heating it to 80 °C. The adsorbent ($c_{adsorbent}$ = 2.5 g L^{-1}) was added, considering this t_0 = 0 min, and the concentration of QN in 2,2,4-trimethylpentane was estimated by UV-Vis after 8 h of contact time.

Experiments combining simultaneous adsorption and extraction were also evaluated, following a similar procedure described above. The QN solution ($[QN]_0^{oil}$= 1000 mg L^{-1}, $[N]_0^{oil}$ = 108 mg L^{-1}) was placed in a reaction vessel and heated to 80 °C. The desired volume of ultrapure water at pH 3.0, not buffered, at 80 °C and considering an O/W ratio = 80:20, was added immediately, followed by the adsorbent ($c_{adsorbent}$ = 2.5 g L^{-1}, considering the total volume of the system), this being t_0 = 0 min. QN concentration, both in oil and water phases, was measured by UV-Vis after 8 h of contact time.

2.4.2. Selective biphasic oxidation: an oxidative denitrogenation (ODN) case study

A QN solution ($[QN]_0^{oil}$ = 1000 mg L^{-1}, $[N]_0^{oil}$ = 108 mg L^{-1}) in 2,2,4-trimethylpentane was placed in a reaction vessel and heated to 80 °C. Upon reaching the desired temperature, a volume of a H_2O_2 solution ($[H_2O_2]_0$ = 247 g L^{-1}) at pH 3.0 (not buffered) and 80 °C was added to achieve an oil-to-water (O/W) volume ratio of 80:20. Around 2–3 min were waited before adding the catalyst (c_{cat} = 2.5 g L^{-1}, considering the whole volume of the system), representing the beginning of the reaction (t_0 = 0 min). Samples were periodically withdrawn to monitor the concentration of QN in oil ($[QN]^{oil}$) and water ($[QN]^{water}$) phases (GC-FID and HPLC, respectively) and H_2O_2 in the water phase (UV-Vis). Samples were collected by respecting the O/W ratio to avoid altering the phase equilibria, and the total amount removed from the reaction during sampling was maintained below 10 % in volume. By the end of the reaction, the catalyst was separated from the liquid medium, and the oily and water phases were stored separately. The water phase was further analyzed in terms of total organic carbon (TOC) content. The catalyst was dried at 60 °C overnight and reused. A non-catalytic run was also conducted without a catalyst, and oxidation reactions in the absence of the pollutant were also carried out to evaluate the possible oxidation of 2,2,4-trimethylpentene; negligible oxidation was observed. Possible carbon leaching from the CNTs was estimated by measuring the TOC content of pure hydrogen peroxide decomposition under aqueous phase only and similar ODN conditions (80 °C, $[H_2O_2]$ = 247 g L^{-1}, [cat] = 2.5 g L^{-1}). The reactions were followed for 24 h in total.

ODN was also carried out for a simulated fuel containing (i) pyridine (PYR) with a concentration of $[PYR]_0^{oil}$ = 610 mg L^{-1} (equivalent to $[N]_0^{oil}$ = 108 mg L^{-1}) in 2,2,4-trimethylpentane, and (ii) a mixture of QN and PYR with a concentration of $[QN]_0^{oil}$ = 500 mg L^{-1} ($[N]_0^{oil}$ = 54 mg L^{-1}) and $[PYR]_0^{oil}$ = 305 mg L^{-1} ($[N]_0^{oil}$ = 54 mg L^{-1}), amounting to a total of $[N]_0^{oil}$ = 108 mg L^{-1}. Reutilization runs were also conducted for MIX-800@Fe for up to 5 cycles. The same procedure described above was followed for each one of the cases, and the reaction was allowed to continue for 1 h when the phases were separated and stored. The catalyst was recovered with a membrane filter (pore: 0.45 μm), washed with distilled water and ethanol, and dried overnight at 105 °C.

2.4.3. Analytical techniques

H_2O_2 concentration was determined by $TiOSO_4$ methodology and measured using UV-Vis (UV–VIS Spectrometer, T70, PG Instrument Ltd) at 405 nm, as described in previous works [44,45]. During extraction and adsorption runs, QN concentration was estimated using UV-Vis at 313 nm for oily ($[QN]^{oil}$) and aqueous ($[QN]^{water}$) phases. For ODN reactions, the concentration of QN was followed by HPLC for the water phase and GC-FID for the oily phase. The separation of QN and reaction products in the water phase was achieved by a JASCO HPLC system coupled to a Nucleosil 100–5C18 (150x2.1 mm) column. An isocratic mobile phase (20 % acetonitrile and 80 % phosphate buffer solution (17 mmol) at pH 6.5) was delivered by a quaternary gradient pump (PU-2089) with a flow rate of 0.5 mL min^{-1}. Detection was achieved in a UV-Vis detector (UV-2075) at 313 nm. The detection of QN in the oily phase was performed in a GC-FID coupled with a SupelcoWax10 column. The oven temperature was set to 40 °C for 10 min, followed by a 10 °C min^{-1} ramp up to 210 °C (hold for 2 min). Detection was set to 200 °C and injection to 250 °C. TOC was measured in a TOC-L (Shimadzu) equipment.

2.4.4. Calculations

QN concentration was monitored throughout the ODN runs by HPLC and GC-FID for water and oily phases, respectively, and the concentrations obtained were transformed into the number of mols, according to Eq. (1).

$$n_{QN_t}^{i} = \frac{[QN]_t^i V^i}{MM_{QN}} \quad (1)$$

where *i* can be either the oil (*i = oil)* or aqueous (*i = water*) phase, $n_{QN_t}^{i}$ is the number of mols of QN at the time *t* and the phase *i* (in μmol), $[QN]_t^i$ is the concentration of QN at time *t* in phase *i* (in g L^{-1}), V^i is the volume of phase *i* (in L), and MM_{QN} is the molar mass of QN (in g mol^{-1}). The total number of mols of QN for each reaction time ($n_{QN_t}^{total}$) was calculated according to Eq. (2) and the total conversion of QN according to Eq. (3):

$$n_{QN_t}^{total} = n_{QN_t}^{water} + n_{QN_t}^{oil} \quad (2)$$

$$X_{QN,total} = \left(1 - \frac{n_{QN_t}^{total}}{n_{QN_0}^{total}}\right) \times 100 \quad (3)$$

in which $X_{QN,total}$ is the global conversion of QN, accounting for both QN in oily and aqueous phase (in %) and $n_{QN_0}^{total}$ is the number of mols of QN at the beginning of the reaction (*t = 0 min*) in both phases (in mol). The

conversion of TOC was calculated according to Eq. (4):

$$TOC_{conversion}(\%) = \left(1 - \frac{(TOC^{water}_{measured} + \mathrm{TOC}^{oil}_{QN})}{TOC_{QN,0}}\right) \times 100 \quad (4)$$

in which $TOC^{water}_{measured}$ is the TOC measured in the water phase by the end of the reaction (in mg L^{-1}), TOC^{oil}_{QN} is the TOC contribution arising from QN still in the oil phase (obtained based on the concentration of QN calculated by GC-FID) (in mg L^{-1}), and $TOC_{QN,0}$ is the TOC contribution from the QN in the beginning of the process (obtained based on the concentration of QN as determined by GC-FID and HPLC for oil and water phases, respectively) (in mg L^{-1}).

A kinetic modeling of the biphasic oxidation reactions was carried out. The methodology considered is based on previous reports on the catalytic wet peroxide oxidation (in the aqueous phase) of phenol [46] and the biphasic oxidation of 2-nitrophenol [23]. The disappearance rate of each species *j* ($-r_j$) in mol h^{-1} is given by Eq. (5):

$$-r_j = \frac{1}{W_{cat}} \bullet \frac{dn_j}{dt} \quad (5)$$

in which n_j is the mols of compound *j* (calculated according to Eq. (1)) and W_{cat} is the mass of the catalyst (in g). The solution of the rate equations and estimation of kinetic parameters was achieved by minimizing the sum of squared errors (SSE_{model}), which was calculated based on the relative number of mols of each species ($n_j/\ n_{j,0}$) for experimental (*exp*) and predicted (*model*) values, according to Eq. (6):

$$SSE_{model} = \sum_{n=1}^{N} \left[\left(\frac{n_j}{n_{j,0}}\right)_{\exp} - \left(\frac{n_j}{n_{j,0}}\right)_{model} \right]^2 \quad (6)$$

Kinetic models were evaluated by the coefficient of determination (R^2) and parity plots.

3. Results and discussion

3.1. Materials characterization

The XRD diffractogram of the CVD catalyst (Fe-NPs/Al_2O_3) is shown in Fig. 1. Two iron phases and two alumina phases were identified in the sample: hematite (Fe_2O_3, COD reference card 96–900–9783) and magnetite (Fe_3O_4, COD reference card 96–900–2318) corresponding to 19 % and 3 % of the sample (semi-quantitative analysis), and α- and γ-alumina (COD reference cards 96–201–5531 and 96–152–8248, respectively), corresponding to 26 % and 52 % of the sample, respectively. Crystallite sizes were estimated using Halder-Wagner and size strain plot, calculated as reported elsewhere [40,47], with hematite estimated to be 9.17 and 9.83 nm, respectively. The content of Fe determined by atomic absorption of the digested sample resulted in iron content of 15 wt% (which corresponds to approximately 21 wt% of hematite).

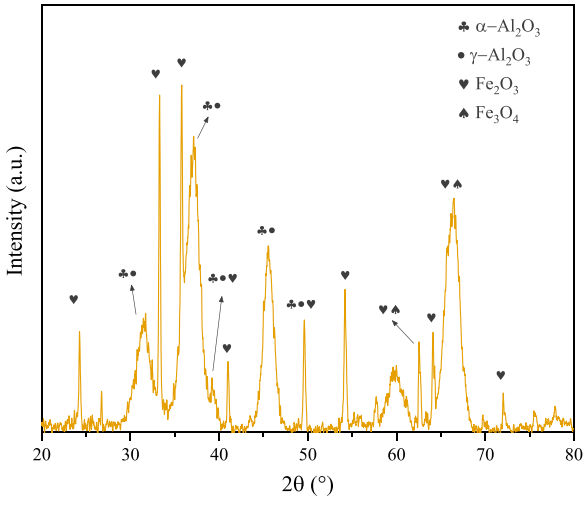

Fig. 1. XRD of Fe-NPs/Al_2O_3.

The morphology of the CNMs obtained in this work is reported in Fig. 2. As observed, LDPE-600@Fe did not result in the growth of a CNT structure, whereas all materials synthesized at 800 °C did result in filamentous structures. All the CNT samples have straight walls in the range of 25–27 walls, which resulted in outer diameters in the same range (26 – 33 nm).

The Raman spectra of the samples are shown in Fig. 3. All spectra have two evident peaks: one centered at 1342 cm^{-1} (D band) and the other at 1600 cm^{-1} (G band). The first peak is ascribed to defects in the carbon structure [48], and the second one is caused by the in-plane stretching of sp^2 carbon atoms, indicating a graphitic nature [49]. A third peak centered at 2700 cm^{-1} was also found for the samples obtained at higher temperatures. This peak is characteristic of CNTs and is associated with the π band in the electronic structure [48]. LDPE-600@Fe did not display this peak as it did not allow the formation of CNTs, as seen in TEM images (Fig. 2). The D/G ratio estimated from the normalized Raman spectra is displayed in Table 1. LDPE-600@Fe has a very high D/G ratio, indicating it to be a highly disordered material. MIX-800@Fe results in slightly disordered materials (D/G ratio of 0.86), whereas the samples synthesized using single polymers all result in more ordered materials (D/G = 0.49–0.67). Similar results have been reported for as-synthesized CNTs derived from plastic solid waste [49,50] and for acid-treated CNTs [51,52].

The contact angles of water with the carbonaceous samples and catalysts used for their preparation are reported in Table 1. Most of the carbon samples synthesized in this work displayed similar values for the water contact angle (123–139°). LDPE-600@Fe and MIX-800@Fe resulted in slightly lower contact angles (123–124°), likely due to higher incorporation of oxygenated compounds. Similar results have been reported for acid-treated CNTs [24,53]. The metal substrate (Fe-NPs/Al_2O_3) used as a CVD catalyst displayed a contact angle of 96°. Higher contents of hematite, as opposed to other iron oxide phases, have been correlated to higher contact angles [54,55].

Table 1 also reports the values obtained for acidic and basic groups in the different samples. LDPE-600@Fe resulted in the highest incorporation of acidic groups (1277 μmol g^{-1}), followed by MIX-800@Fe (632 μmol g^{-1}), which corroborates previously observed characteristics of the materials, such as the presence of amorphous and defective phases in LDPE-600@Fe as seen in TEM images and Raman spectra. Basic groups are within the same range (194–319 μmol g^{-1}) regardless of the sample. All the synthesized materials display magnetic response in the presence of a strong neodymium magnet (Figure S2), whereas Fe-NPs/Al_2O_3 does not.

The TGA data obtained under N_2 atmosphere are displayed in Figure S3. As expected, the materials synthesized at 800 °C are far more stable than the sample obtained at 600 °C. The proximate analysis of the samples is displayed in Table 2. The materials synthesized at 800 °C resulted in a higher content of fixed carbon and lower ashes compared to the sample prepared at 600 °C, especially for HDPE, PP and MIX precursors. HDPE and PP precursors also resulted in a lower content of volatiles. Moisture content was similar for all samples, with a slightly higher value for LDPE-600@Fe (probably associated with the incorporation of surface groups). The ultimate analysis revealed an increased concentration of H and O in LDPE-600@Fe compared to the remaining samples (Table 2), corroborating previous characterizations. Samples synthesized at 800 °C resulted in a similar incorporation of H (H/C ratio in the range 0.003–0.005) and O (O/C ratio in the range 0.010–0.023).

The iron content in the ashes of the CNT samples (Fe_{ashes}) was also calculated (Table 2). As can be seen, materials synthesized at 800 °C resulted in a similar value (59.8–68.3 %), indicating that alumina is removed at a higher rate from the samples during acid washing, as iron

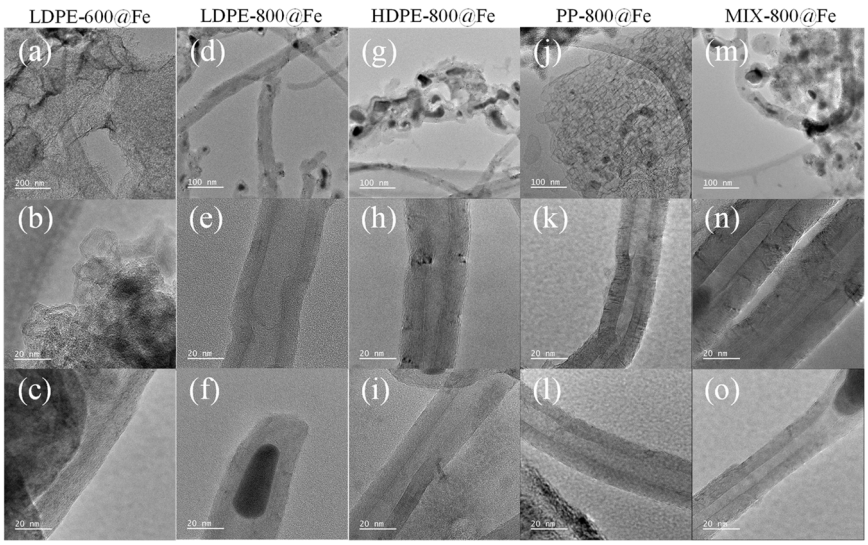

Fig. 2. TEM-photographs of (a-c) LDPE-600@Fe, (d-f) LDPE-800@Fe, (g-i) HDPE-800@Fe, (j-l) PP-800@Fe, and (m-o) MIX-800@Fe nanomaterials.

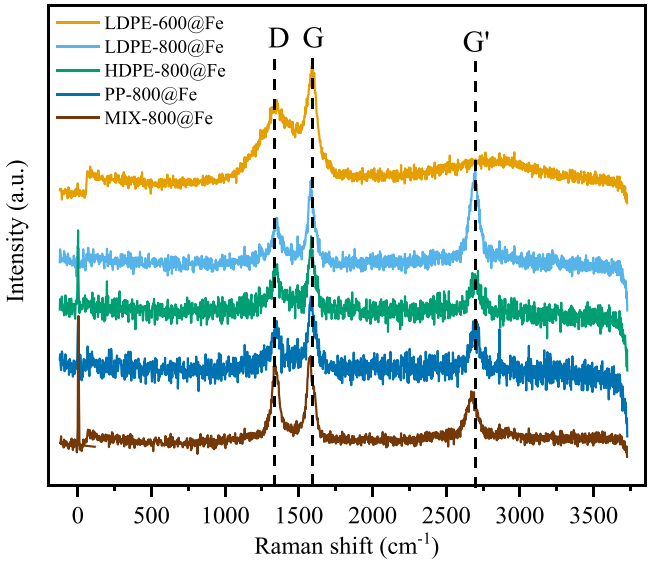

Fig. 3. Raman spectra of the nanomaterials synthesized in this work.

nanoparticles are mainly encapsulated within the walls of the CNTs. The sample LDPE-600@Fe resulted in a lower iron content, likely due to poorer encapsulation of the Fe-NPs during CVD synthesis, and thus, resulting in higher removal of particles located in the outer surface during the acid washing process.

3.2. Denitrogenation process

3.2.1. Extraction and adsorption as blank runs

The extraction of QN from 2,2,4-trimethylpentane, considering ultrapure water at a pH of 3.0 as the extractant phase and different initial QN concentrations, is depicted in Fig. 4(a). As observed, the extraction effect is more relevant for lower initial concentrations regardless of the contact time. For an initial concentration of 250 mg L^{-1}, up to 25 % of QN is removed purely by extraction in 8 h. In contrast, when increasing the concentration to 500 mg L^{-1}, the effect reduces to 16 %. For concentrations over 750 mg L^{-1}, only 7 % of QN is removed by pure extraction in 8 h under the studied conditions. It is also possible to observe that the removal of QN reaches a maximum at around 30 min of contact time, slightly decreasing after up to 8 h, as it reaches an

Table 1
Water contact angles, acidic/basic groups and D/G ratio for the materials used in this work.

Material	Water contact angle	Representative image	Acidic groups (μmol g^{-1})	Basic groups (μmol g^{-1})	D/G ratio
LDPE−600@Fe	124 ± 2°		1277	194	3.46
LDPE−800@Fe	136 ± 2°		197	301	0.67
HDPE−800@Fe	137 ± 1°		137	262	0.49
PP−800@Fe	139 ± 3°		276	271	0.59
MIX−800@Fe	123 ± 7°		632	184	0.86
Commercial CNT	139 ± 4°		291	319	-
Fe-NPs/Al_2O_3	96 ± 4°		742	498	-
Al_2O_3	15 ± 4°		1836	1270	-

Table 2
Proximate analysis of the carbon nanomaterials produced in this work.

Material	Moisture (%)	Volatile content (%)[a]	Ashes (%)[b]	Fixed carbon (%)[c]	H/C ratio	O/C ratio	Fe_{ashes} (%)
LDPE−600@Fe	0.5	24.5	28.0	46.9	0.025	0.064	34.6
LDPE−800@Fe	0.2	19.8	18.0	59.0	0.004	0.010	62.8
HDPE−800@Fe	0.2	15.1	20.5	64.2	0.003	0.010	68.3
PP−800@Fe	0.2	13.2	18.0	65.6	0.005	0.014	66.1
MIX−800@Fe	0.3	10.7	24.9	64.1	0.004	0.023	59.8

[a] determined from TGA in N_2 atmosphere;
[b] determined from TGA in air atmosphere, reported in [21];
[c] calculated as 100-ashes-moisture-volatiles.

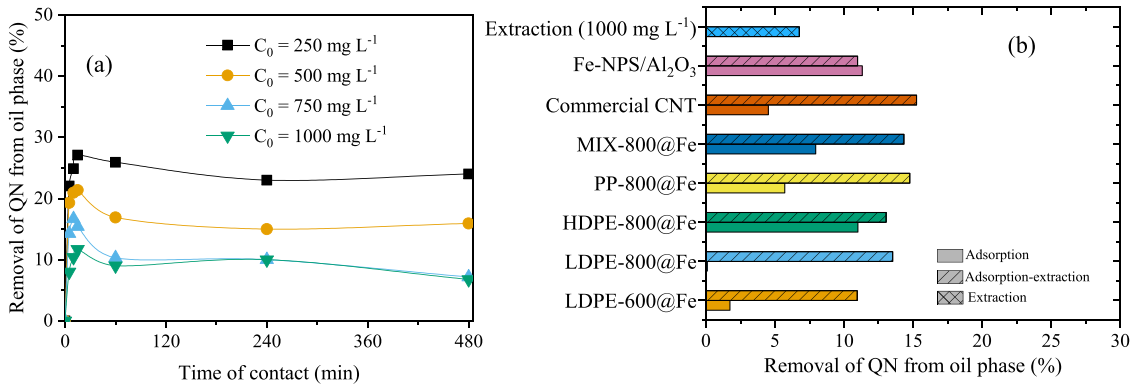

Fig. 4. QN removed from oil phase (a) by pure extraction effect (without catalysts), considering varying initial concentrations of QN; and (b) by pure adsorption (solid filling) and combined adsorption-extraction (patterned filling) in the presence of CNTs and CVD substrate after 8 h of contact time (Conditions: O/W volume ratio = 80:20 (where applicable), pH_0 = 3.0, T = 80 °C; and for adsorption runs: $[QN]_0$ = 1000 mg L^{-1}, $c_{adsorbent}$ = 2.5 g L^{-1}).

equilibrium. The extractions were not carried out for longer than 8 h, as we did not aim to establish the equilibrium between the phases. Rather, we wanted data to compare with the results obtained on oxidation reactions.

Similarly, the removal of QN by pure adsorption after 8 h of contact time, given in Fig. 4(b) (solid filling), ranges between 1 % and 11 %, with the highest removal obtained in the presence of HDPE-800@Fe and Fe-NPs/Al_2O_3 (11 % for both). No other reports were found regarding the adsorption of QN by CNTs. Typical values for the adsorption of other *N*-compounds by CNTs under similar conditions have been reported, such as 14–25 % [22] and 7–13 % [23] for 4-nitrophenol and 2-nitrophenol, respectively, and 11–30 % [20] for paracetamol.

The combined effects of both techniques, *i.e.*, simultaneous extraction and adsorption, were also evaluated, and the obtained results are shown in Fig. 4(b) (patterned filling). It is possible to observe a slight increment in the removal of QN: in all cases, the removal exceeds 10 %; however, neither approach is suitable to remove QN from a simulated fuel, especially for higher concentrations (>750 mg L^{-1}). For comparison purposes, the pure extraction effect after 8 h of contact time for an initial concentration of QN of 1000 mg L^{-1} is also given in Fig. 4(b).

3.2.2. *Oxidative denitrogenation (ODN) of QN*

The results related to the removal of QN under a biphasic system are reported in Fig. 5. The non-catalytic (N.C.) run did not result in significant removal of QN from the fuel, with around 11 % removal in 24 h, similar to the values observed in pure extraction experiments. On the other hand, all CNTs displayed high catalytic activity towards the removal of QN by ODN; complete removals from the fuel are obtained in 60–240 min of reaction, depending on the catalyst, at the selected operating conditions. In the presence of MIX-800@Fe and LDPE-600@Fe, complete removal of QN was observed in only 60 min of reaction, followed closely by HDPE-800@Fe and PP-800@Fe (ca. 90 % in 60 min, and complete removal in less than 4 h), and by Fe-NPs/Al_2O_3, CNT-C and LDPE-800@Fe. Interestingly, it is possible to observe that for all reactions, the reported values start at around 7 % of removal (at time *t = 0 min*). The addition of the extractant phase took place before the addition of the CNTs; thus, this initial removal is solely due to the extraction effect, and the values agree with those reported earlier for the pure extraction effect for an initial concentration of 1 g L^{-1} (Fig. 4(a)). The results reported here (37–100 % of QN removal in 60 min of reaction) for the removal of QN from a simulated fuel fall within the same range as reported in the literature (Table S1) [22,23,26–29,56], with QN removals being reported in the range between 30 % and 100 %, obtained in 30–60 min of reaction. Nevertheless, it should be emphasized that the present work has reported a lower catalyst and hydrogen peroxide concentration than the remaining works dealing with QN. Furthermore, the use of polyolefin-derived CNTs is advantageous from an environmental point of view.

The decomposition of the oxidant during ODN is shown in Fig. 5(b). As can be observed, Fe-NPs/Al_2O_3 and CNT-C resulted in very fast decomposition of the oxidant, especially in the first 1 h of reaction, achieving over 80 % of oxidant consumption. The fast decomposition of hydrogen peroxide allied to the poor ability to adsorb QN in the presence of these materials indicates that there is likely recombination of hydroxyl radicals into non-active species [57], hindering the abatement of QN. On the other hand, the materials LDPE-600@Fe, MIX-800@Fe, PP-800@Fe and HDPE-800@Fe all resulted in around 10 % consumption of the oxidant in 1 h of reaction, which is a sufficient amount of oxidant for QN degradation. The controlled decomposition of H_2O_2 allows for more efficient oxidant usage, translating into a higher QN removal. Notably, an active catalyst, which is also capable of consuming only the required H_2O_2, is crucial for peroxide oxidation systems since H_2O_2 can be the highest operational cost of the process [58]. As far as we are aware, no other works report the consumption of oxidant sources; however, we believe it is crucial to understand better and design the ODN reaction.

QN in the water phase was followed by HPLC, and the results are given in Fig. 5(c). In the presence of HDPE-800@Fe, PP-800@Fe, LDPE-

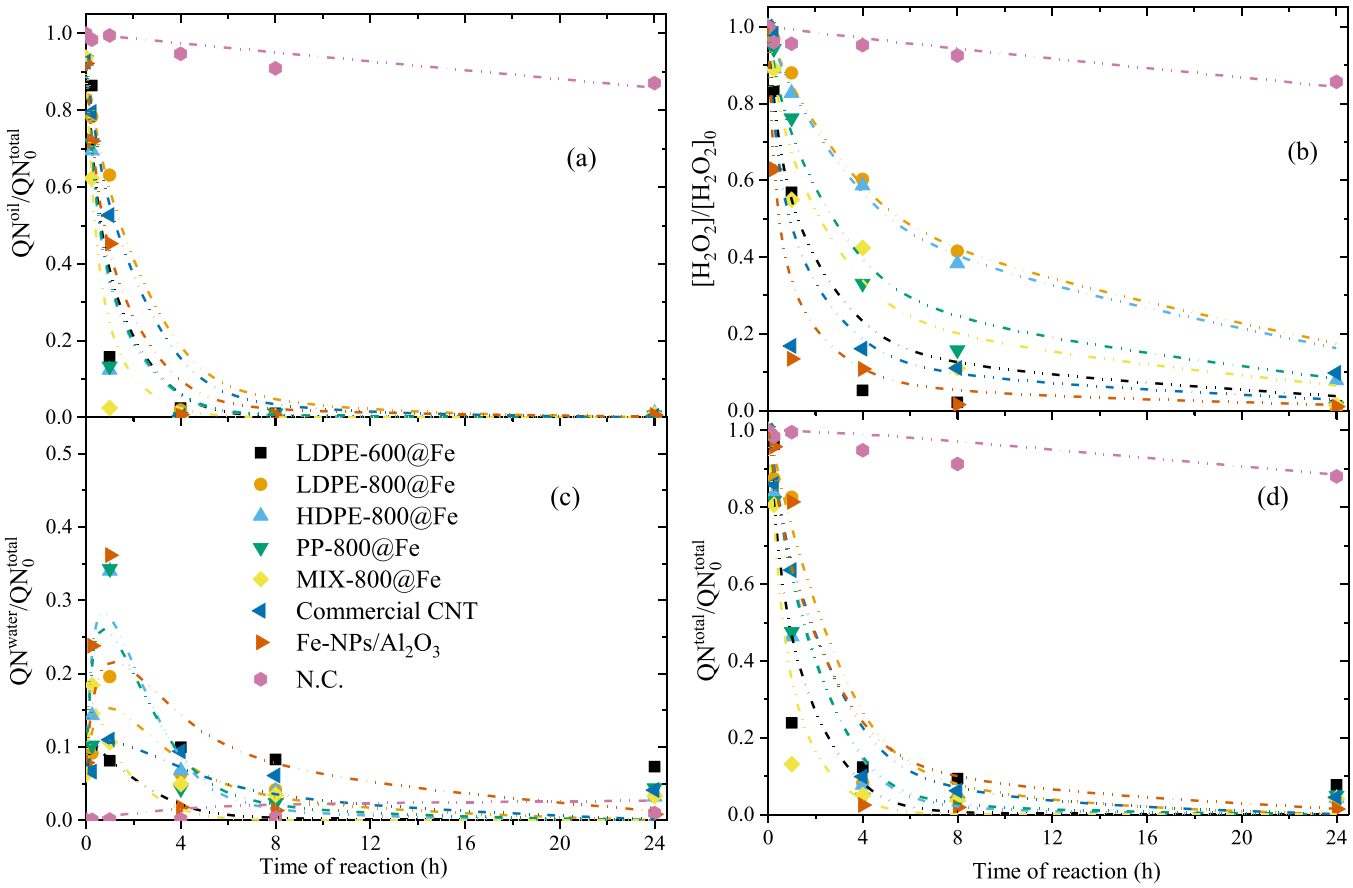

Fig. 5. (a) Normalized number of mols of QN in the oily phase, (b) normalized concentration of H_2O_2 during ODN, (c) normalized number of mols of QN in the water phase, and (d) normalized conversion of total amount of QN during ODN in the presence of the catalysts tested in this work. Conditions: V_{total} = 100 mL, O/W volume ratio = 80:20, pH_0 = 3.0, $[QN]_0^{oil}$ = 1000 mg L^{-1}, c_{cat} = 2.5 g L^{-1}, T = 80 °C, $[H_2O_2]_0$ = 247 g L^{-1}. Dashed lines are from the kinetic model described in Section 3.2.3.

800@Fe and Fe-NPs/Al_2O_3, QN accumulates in the water phase, reaching a maximum at 1 h of reaction, followed by a fast decrease in the next 2 h. In the presence of MIX-800@Fe, QN reaches its maximum in the water phase at a shorter reaction time (15 min). For the remaining materials (LDPE-600@Fe and commercial CNT), not much accumulation of QN is observed. By the end of the reaction, QN is still present in the water phase in most cases, accounting for 1–12 % of QN initially loaded in the system.

The normalized concentration of QN, accounting for QN present both in oil and water phases, is displayed in Fig. 5(d) and follows a similar pattern to that observed for the removal of QN from the oil phase. LDPE-600@Fe and MIX-800@Fe both resulted in the fastest total conversion of QN, reaching more than 80 % of conversion in just 1 h of reaction. In the sequence, PP-800@Fe and HDPE-800@Fe both resulted in over 50 % of QN degradation in 1 h of reaction, followed by CNT-C (35 % in 1 h), Fe-NPs/Al_2O_3 and LDPE-800@Fe (15 % in 1 h). The N.C. run resulted in less than 1 % of QN degradation. In general, for catalyzed reactions, more than 90 % of QN initially loaded was completely degraded in just 2 h of reaction.

The TOC conversion is shown in Fig. 6. As can be observed, most of the materials synthesized in this work display a similar TOC conversion (24–26 %). The CVD-catalyst performs slightly worse (16 %), followed by the commercial CNT sample (11 %). The N.C. run did not allow any significant removal (<1 %), similar to the removals observed for QN itself. The results reported here for TOC conversion are lower than the removals reported for aqueous-phase QN oxidation [21,59,60]. No other works report the TOC conversion for ODN reactions. The results are within the range observed for the removal of other nitrogenated compounds under biphasic systems [22].

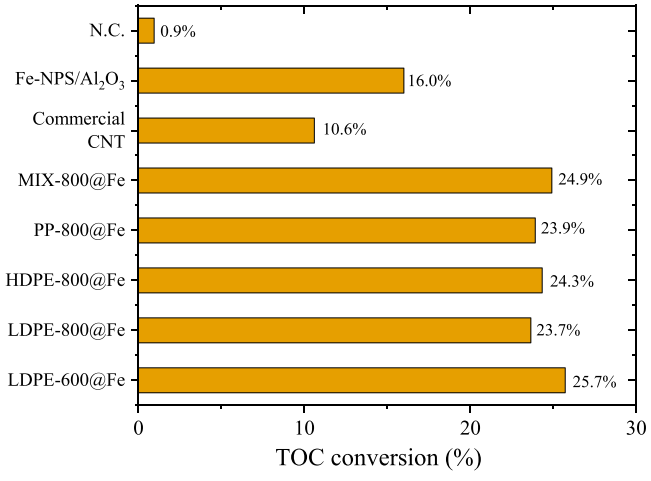

Fig. 6. TOC conversion in the presence of the materials tested in this work. (V_{total} = 100 mL, O/W volume ratio = 80:20, pH_0 = 3.0, $[QN]°_0$ = 1000 mg L^{-1}, c_{cat} = 2.5 g L^{-1}, T = 80 °C, $[H_2O_2]_0$ = 247 g L^{-1}, 24 h of reaction).

Considering the interesting results reported with sample MIX-800@Fe and the fact that it is a sample obtained from a polymer mixture representative of real mixed PSW, MIX-800@Fe was chosen for further testing.

3.2.3. Kinetic modelling and mechanism

The kinetic model described in Text S1 was adjusted to the experimental data, resulting in the kinetics and statistical parameters shown in Table 3. All models adjusted well to the data, as shown by the high coefficient of correlation ($R^2 > 0.94$) and parity plot (Figure S4). The model can also accurately reproduce the experimental data, as shown in Fig. 4(a-d).

The highest kinetic coefficient for the decomposition of hydrogen peroxide was found for Fe-NPs/Al_2O_3, followed by the commercial CNT, LDPE-600@Fe, MIX-800@Fe, PP-800@Fe, HDPE-800@Fe and LDPE-800@Fe. The coefficient for the decomposition of hydrogen peroxide (k_{H2O2}) was found to positively correlate with the O/C ratio for polyolefin-derived CNTs (Figure S5), indicating that the presence of oxygenated groups accelerates the decomposition of H_2O_2. The kinetic constant for QN oxidation follows a different order, with LDPE-600@Fe (66.54 mol^{-1} h^{-1}), MIX-800@Fe (47.46 mol^{-1} h^{-1}) and commercial CNT (45.39 mol^{-1} h^{-1}) displaying significantly higher coefficients compared to the remaining CNTs (<14 mol^{-1} h^{-1}). In all cases, $k'_{QN,ox}$ was higher than $k'_{QN,mt}$, indicating that the mass transfer of QN from the oil phase to the aqueous phase is the limiting step. It should be noted that the materials allowed an increase in $k'_{QN,mt}$ (> 0.55 h^{-1}) compared to the non-catalytic run ($k'_{QN,mt}$ = 0.01 h^{-1}), indicating that their presence facilitates the mass transfer of QN and they indeed act as phase transfer catalysts and are crucial for ODN purposes. The highest $k'_{QN,mt}$ was found for MIX-800@Fe, explaining its more suitable behavior for the process compared to the other samples synthesized at 800 °C. No clear correlation between the materials' characteristics and their ability to act as phase transfer catalysts was found, so this behavior can be attributed to a combination of different characteristics (such as contact angle, oxygenated groups, etc.).

Given the results obtained and the adjusted kinetic model, we propose an expected reaction mechanism, shown in Figure S6. QN is a molecule with a partition coefficient (logP) that is highly affected by the pH of the aqueous phase [61], as pH affects the dissociation of QN. At pHs lower than its p*K*a (approximately 4.9), more QN is expected to migrate to the water phase [61], and its solubility in water increases [62]. Under the conditions studied in this work, we expect that QN initially migrates to the water phase (as observed in extraction experiments and represented in Figure S6, I), especially since the reactions were carried out under an acidic pH. The addition of the CNTs (Figure S6, II) can further enhance the mass transfer of QN to the water phase (Figure S6, IIa) given that the CNTs can act as phase transfer catalysts, as shown by the increased $k'_{QN,mt}$ (> 0.55 h^{-1}) in comparison to the non-catalytic run ($k'_{QN,mt}$ = 0.01 h^{-1}). The CNTs also are responsible for yielding hydroxyl radicals (Figure S6, IIIa), leading to the oxidation of QN (Figure S6, III and IIIa); we expect that QN both in water, oil and interface between phases to be oxidized, although the QN present in the aqueous phase is the most likely to be oxidized. Given that the mass transfer of QN was found to be the limiting step, more effective materials, such as MIX-800@Fe, should address this issue. The degradation of QN in the water phase disrupts the equilibrium of QN between the oil and aqueous phase, resulting in more QN migrating towards the water phase (Figure S6, IV). This extraction-oxidation-extraction cycle (Figure S6, III ↔ IV) will continue until all QN is removed from the oil phase (Figure S6, V). Since the products formed are more hydrophilic, they are expected to remain in the water phase (Figure S6, V). It is also important to note that oxidized intermediates can be further degraded into other oxidized compounds until reaching refractory compounds (such as low-molecular-weight carboxylic acids [63]) and ultimately full mineralization products (CO_2 and H_2O). It should be noted that the selectivity towards degradation of QN or intermediates depends on several factors, especially the materials' adsorptive interactions with each intermediate.

3.2.4. ODN of PYR and mixtures of PYR and QN

MIX-800@Fe was tested as a catalyst in the ODN of PYR or QN (as individual compounds) and benchmarked against the commercial CNT. The results are reported in Fig. 7. The removal of PYR was superior in the presence of the sample prepared from a mix of polyolefins (MIX-800@Fe) compared to commercial CNT. In 1 h of reaction, nearly 87 % of PYR was removed from the fuel phase in the presence of MIX-800@Fe compared to 69 % for commercial CNT. Relating to the quinoline abatement, QN removal achieved 98 and 47 % with MIX-800@Fe and commercial CNT under the same timeframe, respectively. The higher activity of MIX-800@Fe compared to the commercial CNT sample for the selective oxidation of PYR may be ascribed to its ability to act as a phase transfer catalyst (as seen in Table 3). As previously performed for QN removal, pure extraction by water and adsorption of PYR on the catalyst were studied under the same operating conditions. In the case of PYR, pure extraction accounts for a high proportion of PYR (nearly 50 %, Fig. 7). The higher extraction effect for PYR is related to its lower logP compared to QN (0.65 for PYR [64] and 2.03 for QN [65] at neutral pH). Pure adsorption accounts for 3.2 and 2.8 % with MIX-800@Fe and commercial CNT, respectively. Combined adsorption and extraction

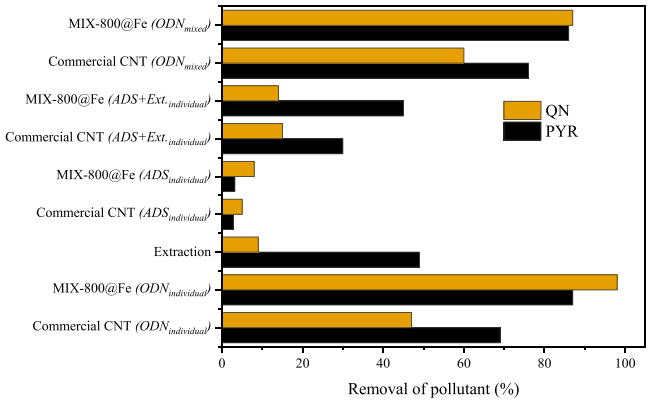

Fig. 7. Removal of QN or PYR from the oily phase during ODN in the presence of commercial CNT and MIX-800@Fe after 60 min of reaction considering the components individually ($ODN_{individual}$) and in a mixture (ODN_{mixed}). (V_{total} = 100 mL, O/W volume ratio = 80:20, pH_0 = 3.0, $[QN]_0^{oil}$ = 1000 mg L^{-1} or $[PYR]_0^{oil}$ = 610 mg L^{-1} (in runs with mixed fuel: $[QN]_0^{oil}$ = 500 mg L^{-1} and $[PYR]_0^{oil}$ = 305 mg L^{-1}), c_{cat} = 2.5 g L^{-1}, T = 80 °C, $[H_2O_2]_0$ = 247 g L^{-1}, 1 h).

Table 3
Kinetic and statistical coefficients obtained from the fit of the kinetic model (Text S1) during ODN.

Coefficient	LDPE-600@Fe	LDPE-800@Fe	HDPE-800@Fe	PP-800@Fe	MIX-800@Fe	Commercial CNT	Fe-NPs/Al_2O_3	N.C.
k_{H2O2} (mol^{-1} h^{-1})	7.23	1.33	1.57	3.04	3.97	10.18	18.58	0.05
$k'_{QN,mt}$ (h^{-1})	1.21	0.55	1.44	1.39	2.08	0.63	1.03	0.01
$k_{QN,ox}$ (mol^{-1} h^{-1})	66.54	14.22	12.71	14.43	47.46	45.39	33.08	1.40
POW	0.18							
SSE_{model}	0.103	0.057	0.055	0.067	0.050	0.138	0.066	0.007
R^2	0.958	0.980	0.977	0.974	0.977	0.942	0.967	0.999

represent 30 and 45 % of removal in 1 h with commercial CNT and MIX-800@Fe, respectively, which may indicate some resistance to mass transfer, mainly in the presence of the commercial CNT.

In the case of ODN of a mixed fuel (*ODN* $_{mixed}$ in Fig. 7) containing simultaneously QN and PYR, 87 % and 86 %, respectively, are removed from the fuel phase with MIX-800@Fe. The catalytic activity for the ODN of QN seems to decrease slightly in the presence of PYR. In contrast, PYR removal is unaffected, possibly due to the higher contribution of extraction for PYR. Nevertheless, the overall removal of *N* from the fuel remains high (87 %), indicating that the material is versatile for removing *N*-compounds.

3.2.5. Catalyst reuse

The results obtained for the reutilization runs of MIX-800@Fe are reported in Fig. 8. As can be observed, no obvious loss of catalytic activity was observed for the 6 cycles reported here, maintaining an average removal of QN from the fuel of 98 % in just 1 h of reaction. This indicates that the catalyst is highly stable for the proposed system. Metal leaching was assessed during experiments through atomic absorption and negligible metal leaching from catalyst into aqueous media was observed (<0.05 wt% of MIX-800@Fe). Similarly, carbon loss was assessed by measuring TOC of the aqueous phase for pure hydrogen decomposition reactions under similar ODN conditions, and no carbon was measured in the aqueous phase (<0.5 $mg_C\ L^{-1}$).

4. Conclusions

The feasibility to prepare CNTs by CVD over iron particles supported on alumina was demonstrated at 800 ºC using different individual polymers as carbon precursor, and a mixture representative of the typical composition of plastic solid wastes found in municipal residual streams. The CNTs were applied for the oxidation of QN considering a 2,2,4-trimethylpentane-water to simulate the selective ODN of liquid fuels. The complete removal of QN after 60–240 min was achieved, depending on the CNT catalyst, at the operating conditions of 80 °C, pH of the aqueous phase of 3.0, $c_{cat} = 2.5\ g\ L^{-1}$, O/W volume ratio of 80:20 and $[H_2O_2]_0 = 247\ g\ L^{-1}$. The catalytic activity shown by the materials synthesized in the ODN of QN far surpassed that of the commercial CNT sample. Additionally, the removal of QN by ODN was compared to the removal obtained by water extraction and adsorption with the materials at the same operating conditions, evidencing that QN removals obtained are mainly due to oxidation. In fact, kinetic modelling indicated that the mass transference from oil to aqueous phase is the limiting step in the reaction, and higher removals in the catalyzed runs were ascribed to the ability of the CNTs to act as phase transfers catalysts. For the ODN of QN, over 98 % of the initial content was completely removed for a simulated fuel in 1 h of reaction, and this activity was maintained for up to 5 additional cycles in the presence of the catalyst prepared from a mixture of 35:25:40 of LDPE:HDPE:PP (MIX-800@Fe). MIX-800@Fe could also remove significant amounts of PYR from 2,2,4-trimethylpentane in just 1 h of reaction and PYR and QN when they were simultaneously present. The results reported here suggest that polyolefins are suitable precursors for the synthesis of highly active CNTs for oxidation purposes, and it should prompt further studies into the application of real PSW. The solution proposed here could help increase the sustainability of the removal of N compounds, specifically related to the reintroduction of plastic solid waste into the economy.

CRediT authorship contribution statement

Adriano Santos Silva: Writing – original draft, Visualization, Formal analysis, Data curation. **Jose L. Diaz de Tuesta:** Writing – review & editing, Project administration, Methodology, Funding acquisition, Conceptualization. **Admilson Vieira:** Writing – review & editing. **Adrián M. T. Silva:** Writing – review & editing, Supervision. **Joaquim L. Faria:** Writing – review & editing, Supervision. **Helder T. Gomes:** Writing – review & editing, Supervision, Project administration, Funding acquisition. **Fernanda F. Roman:** Writing – original draft, Visualization, Methodology, Investigation, Formal analysis, Data curation, Conceptualization. **Larissa Piccinin:** Investigation, Formal analysis.

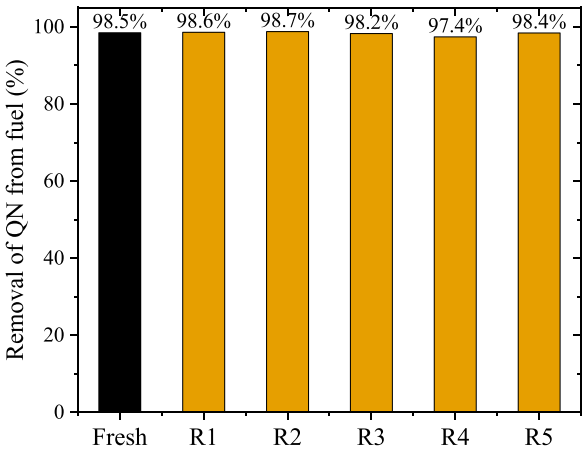

Fig. 8. Removal of QN from the fuel phase in the presence of MIX-800@Fe after 60 min of reaction for fresh catalyst and reutilization runs. Conditions: $V_{total} = 25$ mL, O/W volume ratio = 80:20, $pH_0 = 3.0$, $[QN]^\circ_0 = 1000\ mg\ L^{-1}$ (equivalent to $[N]^\circ_0 = 108\ mg\ L^{-1}$), $c_{cat} = 2.5\ g\ L^{-1}$, T = 80 °C, $[H_2O_2]_0 = 247\ g\ L^{-1}$.

Declaration of Competing Interest

The authors declare that they have no known competing financial interests or personal relationships that could have appeared to influence the work reported in this paper.

Acknowledgments

This work was financially supported by project "PLASTIC_TO_FUEL&MAT – Upcycling Waste Plastics into Fuel and Carbon Nanomaterials" (PTDC/EQU-EQU/31439/2017), CIMO (UIDB/00690/2020) through FEDER under Program PT2020 and by national funds through the FCT/MCTES (PIDDAC): LSRE-LCM, UIDB/50020/2020 (DOI: 10.54499/UIDP/50020/2020) and UIDP/50020/2020 (DOI: 10.54499/UIDP/50020/2020); and ALiCE, LA/P/0045/2020 (DOI: 10.54499/LA/P/0045/2020). Fernanda F. Roman acknowledges the national funding by FCT and the European Social Fund, FSE, through the individual research grant SFRH/BD/143224/2019. Adriano Santos Silva thanks the financial support from FCT under MIT Portugal Program with Ph.D. grant SFRH/BD/151346/2021. J. L. Diaz de Tuesta acknowledges the research grant (2022-T1/AMB-23946) by the program of *Atracción al Talento* of *Comunidad de Madrid* (Spain). The authors are grateful to Sociedade Ponto Verde for the financial support through the project "*Estudo técnico-económico para a valorização de resíduos de embalagens plásticas em nanotubos de carbono*."

Appendix A. Supporting information

Supplementary data associated with this article can be found in the online version at doi:10.1016/j.jece.2024.115128.

Data availability

Data will be made available on request.

References

[1] A. Rajendran, T.-y Cui, H.-x Fan, Z.-f Yang, J. Feng, W.-y Li, A comprehensive review on oxidative desulfurization catalysts targeting clean energy and

environment, J. Mater. Chem. A 8 (5) (2020) 2246–2285, https://doi.org/10.1039/c9ta12555h.
[2] M. Kampa, E. Castanas, Human health effects of air pollution, Environ. Pollut. 151 (2) (2008) 362–367, https://doi.org/10.1016/j.envpol.2007.06.012.
[3] C. Pénard-Morand, I. Annesi-Maesano, Air pollution: from sources of emissions to health effects, Breathe 1 (2) (2004) 108–119.
[4] P. Grennfelt, A. Engleryd, M. Forsius, O. Hov, H. Rodhe, E. Cowling, Acid rain and air pollution: 50 years of progress in environmental science and policy, Ambio 49 (4) (2020) 849–864, https://doi.org/10.1007/s13280-019-01244-4.
[5] D.A. Burns, J. Aherne, D.A. Gay, C.M.B. Lehmann, Acid rain and its environmental effects: recent scientific advances, Atmos. Environ. 146 (2016) 1–4, https://doi.org/10.1016/j.atmosenv.2016.10.019.
[6] M. Hughes, K.C. Jones, M.E. Hums, R.A. Cairncross, V.T. Wyatt, Identification of sulfur-containing impurities in biodiesel produced from brown grease, J. Am. Oil Chem. ' Soc. 95 (4) (2018) 407–420, https://doi.org/10.1002/aocs.12048.
[7] H. Ma, M.M. Addy, E. Anderson, W. Liu, Y. Liu, Y. Nie, P. Chen, B. Cheng, H. Lei, R. Ruan, A novel process for low-sulfur biodiesel production from scum waste, Bioresour. Technol. 214 (2016) 826–835, https://doi.org/10.1016/j.biortech.2016.05.029.
[8] F.F. Roman, J.L. Diaz de Tuesta, A.M.T. Silva, J.L. Faria, H.T. Gomes, Carbon-based materials for oxidative desulfurization and denitrogenation of fuels: a review, Catalysts 11 (10) (2021) 1239, https://doi.org/10.3390/catal11101239.
[9] M.F. Majid, H.F. Mohd Zaid, C.F. Kait, K. Jumbri, L.C. Yuan, S. Rajasuriyan, Futuristic advance and perspective of deep eutectic solvent for extractive desulfurization of fuel oil: a review, J. Mol. Liq. 306 (2020) 112870, https://doi.org/10.1016/j.molliq.2020.112870.
[10] E. Svinterikos, I. Zuburtikudis, M. Al-Marzouqi, Carbon nanomaterials for the adsorptive desulfurization of fuels, J. Nanotechnol. 2019 (2019) 1–13, https://doi.org/10.1155/2019/2809867.
[11] J.G. Speight, N.S. El-Gendy, Biocatalytic Desulfurization, Introd. Pet. Biotechnol. (2018) 165–227, https://doi.org/10.1016/b978-0-12-805151-1.00006-0.
[12] European Commision, Commission proposes new Euro 7 standards to reduce pollutant emissions from vehicles and improve air quality, 2022. Available at https://ec.europa.eu/commission/presscorner/detail/en/ip_22_6495. (Accessed January 24th, 2023 2023).
[13] G.H.C. Prado, Y. Rao, A. de Klerk, Nitrogen removal from oil: a review, Energy Fuels 31 (1) (2017) 14–36, https://doi.org/10.1021/acs.energyfuels.6b02779.
[14] R.G. Faria, D. Silva, F. Mirante, S. Gago, L. Cunha-Silva, S.S. Balula, Advanced technologies conciliating desulfurization and denitrogenation to prepare clean fuels, Catalysts 14 (2) (2024), https://doi.org/10.3390/catal14020137.
[15] S. Kumari, S. Sengupta, Non-hydrogen processes for simultaneous desulfurization and denitrogenation of light petroleum fuels-an elaborative review, Environ. Sci. Pollut. Res Int 28 (44) (2021) 61873–61907, https://doi.org/10.1007/s11356-021-15909-9.
[16] J. Zhao, R. Wang, Research progress of phase transfer catalysts used in oxidative desulfurization of fuel oil, Mini Rev. Org. Chem. 18 (5) (2021) 626–648, https://doi.org/10.2174/1570193x17999200820160851.
[17] Y. Zhou, Z. Guo, W. Hou, Q. Wang, J. Wang, Polyoxometalate-based phase transfer catalysis for liquid–solid organic reactions: a review, Catal. Sci. Technol. 5 (9) (2015) 4324–4335, https://doi.org/10.1039/c5cy00674k.
[18] R.S. Ribeiro, O. Vieira, R. Fernandes, F.F. Roman, J.L. Diaz de Tuesta, A.M.T. Silva, H.T. Gomes, Synthesis of low-density polyethylene derived carbon nanotubes for activation of persulfate and degradation of water organic micropollutants in continuous mode, J. Environ. Manag. 308 (2022) 114622, https://doi.org/10.1016/j.jenvman.2022.114622.
[19] M. Martin-Martinez, B.F. Machado, P. Serp, S. Morales-Torres, A.M.T. Silva, J. L. Figueiredo, J.L. Faria, H.T. Gomes, Carbon nanotubes as catalysts for wet peroxide oxidation: the effect of surface chemistry, Catal. Today 357 (2020) 332–340, https://doi.org/10.1016/j.cattod.2019.03.014.
[20] J.L. Diaz de Tuesta, A.S. Silva, F.F. Roman, L.F. Sanches, F.A. da Silva, A.I. Pereira, A.M.T. Silva, J.L. Faria, H.T. Gomes, Polyolefin-derived carbon nanotubes as magnetic catalysts for wet peroxide oxidation of paracetamol in aqueous solutions, Catal. Today 419 (2023) 114162, https://doi.org/10.1016/j.cattod.2023.114162.
[21] F.F. Roman, L. De Grande Piccinin, A. Santos Silva, J.L. Diaz de Tuesta, I.V. K. Freitas, A. Vieira, G. Gonçalves Lenzi, A.M.T. Silva, J.L. Faria, H.T. Gomes, Carbon nanomaterials from polyolefin waste: effective catalysts for quinoline degradation through catalytic wet peroxide oxidation, Catalysts 13 (9) (2023) 1259, https://doi.org/10.3390/catal13091259.
[22] F.F. Roman, J.L. Diaz de Tuesta, F.K.K. Sanches, A.S. Silva, P. Marin, B.F. Machado, P. Serp, M. Pedrosa, A.M.T. Silva, J.L. Faria, H.T. Gomes, Selective denitrification of simulated oily wastewater by oxidation using Janus-structured carbon nanotubes, Catal. Today (2023) 114001, https://doi.org/10.1016/j.cattod.2023.01.008.
[23] J.L. Diaz de Tuesta, B. F. Machado, P. Serp, A.M. T. Silva, J.L. Faria, H. T. Gomes, Janus amphiphilic carbon nanotubes as Pickering interfacial catalysts for the treatment of oily wastewater by selective oxidation with hydrogen peroxide, Catal. Today 356 (2020) 205–215, https://doi.org/10.1016/j.cattod.2019.07.012.
[24] C. Herrera, L. Barrientos, A. Rosenkranz, C. Sepulveda, J.L. García-Fierro, M. A. Laguna-Bercero, N. Escalona, Tuning amphiphilic properties of Ni/Carbon nanotubes functionalized catalysts and their effect as emulsion stabilizer for biomass-derived furfural upgrading, Fuel 276 (2020) 118032, https://doi.org/10.1016/j.fuel.2020.118032.
[25] A.D. Purceno, B.F. Machado, A.P. Teixeira, T.V. Medeiros, A. Benyounes, J. Beausoleil, H.C. Menezes, Z.L. Cardeal, R.M. Lago, P. Serp, Magnetic amphiphilic hybrid carbon nanotubes containing N-doped and undoped sections: powerful tensioactive nanostructures, Nanoscale 7 (1) (2015) 294–300, https://doi.org/10.1039/c4nr04005h.
[26] A.A.S. Oliveira, A.R. Martins, R.V. Ferreira, I.T. Cunha, P. Serp, J.P. de Mesquita, F. C.C. Moura, N-doped carbon nanotubes grown on red mud residue: Hybrid nanocomposites for technological applications, Catal. Today 344 (2020) 247–258, https://doi.org/10.1016/j.cattod.2019.04.060.
[27] A.A.S. Oliveira, I.F. Teixeira, T. Christofani, J.C. Tristão, I.R. Guimarães, F.C. C. Moura, Biphasic oxidation reactions promoted by amphiphilic catalysts based on red mud residue, Appl. Catal. B-Environ. 144 (2014) 144–151, https://doi.org/10.1016/j.apcatb.2013.07.015.
[28] I.F. Teixeira, A.Ad.S. Oliveira, T. Christofani, F.C.C. Moura, Biphasic oxidation promoted by magnetic amphiphilic nanocomposites undergoing a reversible emulsion process, J. Mater. Chem. A 1 (35) (2013) 10203–10208, https://doi.org/10.1039/c3ta11535f.
[29] R.V. Mambrini, C.Z. Maia, J.D. Ardisson, P.P. de Souza, F.C.C. Moura, Fe/C and FeMo/C hybrid materials for the biphasic oxidation of fuel contaminants, N. J. Chem. 41 (1) (2017) 142–150, https://doi.org/10.1039/c6nj02718k.
[30] [dataset] Eurostat, Packaging waste by waste management operations, 2021. https://doi.org/10.2908/ENV_WASPAC.
[31] [dataset] Eurostat, Recycling rates of packaging waste for monitoring compliance with policy targets, by type of packaging, 2021. https://doi.org/10.2908/ENV_WASPACR.
[32] W.W.Y. Lau, Y. Shiran, R.M. Bailey, E. Cook, M.R. Stuchtey, J. Koskella, C.A. Velis, L. Godfrey, J. Boucher, M.B. Murphy, R.C. Thompson, E. Jankowska, A. Castillo Castillo, T.D. Pilditch, B. Dixon, L. Koerselman, E. Kosior, E. Favoino, J. Gutberlet, S. Baulch, M.E. Atreya, D. Fischer, K.K. He, M.M. Petit, U.R. Sumaila, E. Neil, M. V. Bernhofen, K. Lawrence, J.E. Palardy, Evaluating scenarios toward zero plastic pollution, Science (2020) 1455–1461, https://doi.org/10.1126/science.aba9475.
[33] PlasticsEurope, Plastics - the facts 2020, 2020. Available at https://plasticseurope.org/knowledge-hub/plastics-the-facts-2020/. (Accessed January 20th, 2024).
[34] C. Zhuo, Y.A. Levendis, Upcycling waste plastics into carbon nanomaterials: a review, J. Appl. Polym. Sci. 131 (4) (2014) 39931, https://doi.org/10.1002/app.39931.
[35] O. Vieira, R.S. Ribeiro, J.L. Diaz de Tuesta, H.T. Gomes, A.M.T. Silva, A systematic literature review on the conversion of plastic wastes into valuable 2D graphene-based materials, Chem. Eng. J. 428 (2022) 131399, https://doi.org/10.1016/j.cej.2021.131399.
[36] N. Cai, X. Li, S. Xia, L. Sun, J. Hu, P. Bartocci, F. Fantozzi, P.T. Williams, H. Yang, H. Chen, Pyrolysis-catalysis of different waste plastics over Fe/Al_2O_3 catalyst: high-value hydrogen, liquid fuels, carbon nanotubes and possible reaction mechanisms, Energy Convers. Manag. 229 (2021) 113794, https://doi.org/10.1016/j.enconman.2020.113794.
[37] A. Mukherjee, B. Debnath, S.K. Ghosh, Carbon nanotubes as a resourceful product derived from waste plastic—A review, in: S.K. Ghosh (Ed.), Waste Management and Resource Efficiency, Springer Singapore, Singapore, 2019, pp. 915–934, https://doi.org/10.1007/978-981-10-7290-1_77.
[38] A.A. Aboul-Enein, A.E. Awadallah, A.A.H. Abdel-Rahman, A.M. Haggar, Synthesis of multi-walled carbon nanotubes via pyrolysis of plastic waste using a two-stage process, Fuller. Nanotub. Carbon Nanostruct. 26 (7) (2018) 443–450, https://doi.org/10.1080/1536383x.2018.1447929.
[39] A. Ahamed, A. Veksha, K. Yin, P. Weerachanchai, A. Giannis, G. Lisak, Environmental impact assessment of converting flexible packaging plastic waste to pyrolysis oil and multi-walled carbon nanotubes, J. Hazard Mater. 390 (2020) 121449, https://doi.org/10.1016/j.jhazmat.2019.121449.
[40] A.S. Silva, J.L. Diaz de Tuesta, T. Sayuri Berberich, S. Delezuk Inglez, A.R. Bertao, I. Caha, F.L. Deepak, M. Banobre-Lopez, H.T. Gomes, Doxorubicin delivery performance of superparamagnetic carbon multi-core shell nanoparticles: pH dependence, stability and kinetic insight, Nanoscale 14 (19) (2022) 7220–7232, https://doi.org/10.1039/d1nr08550f.
[41] M.S. Abbas-Abadi, Y. Ureel, A. Eschenbacher, F.H. Vermeire, R.J. Varghese, J. Oenema, G.D. Stefanidis, K.M. Van Geem, Challenges and opportunities of light olefin production via thermal and catalytic pyrolysis of end-of-life polyolefins: towards full recyclability, Prog. Energy Combust. Sci. 96 (2023), https://doi.org/10.1016/j.pecs.2022.101046.
[42] E. Nowak, G. Combes, E.H. Stitt, A.W. Pacek, A comparison of contact angle measurement techniques applied to highly porous catalyst supports, Powder Technol. 233 (2013) 52–64, https://doi.org/10.1016/j.powtec.2012.08.032.
[43] J. Dove, A comparison of two contact angle measurement methods and inverse gas chromatography to assess the surface energies of theophylline and caffeine, Int. J. Pharm. 138 (2) (1996) 199–206, https://doi.org/10.1016/0378-5173(96)04535-8.
[44] A. Santos Silva, M. Seitovna Kalmakhanova, B. Kabykenovna Massalimova, J. G. Sgorlon, Dd.T. Jose Luis, H.T. Gomes, Wet peroxide oxidation of paracetamol using acid activated and fe/co-pillared clay catalysts prepared from natural clays, Catalysts 9 (9) (2019) 705, https://doi.org/10.3390/catal9090705.
[45] A.S. Silva, F.F. Roman, A.V. Dias, J.L. Diaz de Tuesta, A. Narcizo, A.P.F. da Silva, I. Çaha, F.L. Deepak, M. Bañobre-López, A.M.C. Ferrari, H.T. Gomes, Hybrid multi-core shell magnetic nanoparticles for wet peroxide oxidation of paracetamol: application in synthetic and real matrices, J. Environ. Chem. Eng. 11 (5) (2023) 110806, https://doi.org/10.1016/j.jece.2023.110806.
[46] J.L. Diaz de Tuesta, A. Quintanilla, J.A. Casas, J.J. Rodriguez, Kinetic modeling of wet peroxide oxidation with a carbon black catalyst, Appl. Catal. B: Environ. 209 (2017) 701–710, https://doi.org/10.1016/j.apcatb.2017.03.031.
[47] S. Moretto, A. Santos Silva, J.L. Diaz de Tuesta, F. F. Roman, R. Cortesi, A. R. Bertão, M. Bañobre-López, M. Pedrosa, A.M.T. Silva, H.T. Gomes, Comprehensive characterization and development of multi-core shell superparamagnetic nanoparticles for controlled delivery of drugs and their kinetic

release modelling, Mater. Today Chem. 33 (2023), https://doi.org/10.1016/j.mtchem.2023.101748.
[48] R.G. Morais, N. Rey-Raap, J.L. Figueiredo, M.F.R. Pereira, Fe, Co, N-doped carbon nanotubes as bifunctional oxygen electrocatalysts, Appl. Surf. Sci. 572 (2022), https://doi.org/10.1016/j.apsusc.2021.151459.
[49] J. Wang, B. Shen, M. Lan, D. Kang, C. Wu, Carbon nanotubes (CNTs) production from catalytic pyrolysis of waste plastics: the influence of catalyst and reaction pressure, Catal. Today 351 (2020) 50–57, https://doi.org/10.1016/j.cattod.2019.01.058.
[50] D. Yao, H. Yang, Q. Hu, Y. Chen, H. Chen, P.T. Williams, Carbon nanotubes from post-consumer waste plastics: investigations into catalyst metal and support material characteristics, Appl. Catal. B: Environ. 280 (2021), https://doi.org/10.1016/j.apcatb.2020.119413.
[51] H. Liu, J. Wang, J. Wang, S. Cui, Sulfonitric treatment of multiwalled carbon nanotubes and their dispersibility in water, Materials 11 (12) (2018), https://doi.org/10.3390/ma11122442.
[52] N. Mohd Saidi, M.N. Norizan, N. Abdullah, N. Janudin, N.A.M. Kasim, M.J. Osman, I.S. Mohamad, Characterizations of MWCNTs nanofluids on the effect of surface oxidative treatments, Nanomaterials 12 (7) (2022), https://doi.org/10.3390/nano12071071.
[53] N. Briggs, A.K.Y. Raman, L. Barrett, C. Brown, B. Li, D. Leavitt, C.P. Aichele, S. Crossley, Stable pickering emulsions using multi-walled carbon nanotubes of varying wettability, Colloids Surf. A Physicochem. Eng. Asp. 537 (2018) 227–235, https://doi.org/10.1016/j.colsurfa.2017.10.010.
[54] S.M. Iveson, S. Holt, S. Biggs, Contact angle measurements of iron ore powders, Colloids Surf. A: Physicochem. Eng. Asp. 166 (1-3) (2000) 203–214, https://doi.org/10.1016/s0927-7757(99)00455-0.
[55] S.M. Iveson, S. Holt, S. Biggs, Advancing contact angle of iron ores as a function of their hematite and goethite content: implications for pelletising and sintering, Int. J. Miner. Process. 74 (1-4) (2004) 281–287, https://doi.org/10.1016/j.minpro.2004.01.007.
[56] I.R. Guimarães, A.S. Giroto, W.F. de Souza, M.C. Guerreiro, Highly reactive magnetite covered with islands of carbon: oxidation of N and S-containing compounds in a biphasic system, Appl. Catal A-Gen. 450 (2013) 106–113, https://doi.org/10.1016/j.apcata.2012.10.017.
[57] R.S. Ribeiro, A.M.T. Silva, J.L. Figueiredo, J.L. Faria, H.T. Gomes, Catalytic wet peroxide oxidation: a route towards the application of hybrid magnetic carbon nanocomposites for the degradation of organic pollutants. A review, Appl. Catal. B: Environ. 187 (2016) 428–460, https://doi.org/10.1016/j.apcatb.2016.01.033.
[58] J.L. Diaz de Tuesta, A. Quintanilla, D. Moreno, V.R. Ferro, J.A. Casas, Simulation and optimization of the CWPO process by combination of aspen plus and 6-factor doehlert matrix: towards autothermal operation, Catalysts 10 (5) (2020), https://doi.org/10.3390/catal10050548.
[59] L. Chu, J. Wang, J. Dong, H. Liu, X. Sun, Treatment of coking wastewater by an advanced Fenton oxidation process using iron powder and hydrogen peroxide, Chemosphere 86 (4) (2012) 409–414, https://doi.org/10.1016/j.chemosphere.2011.09.007.
[60] D. Liu, C. Wang, Y. Song, Y. Wei, L. He, B. Lan, X. He, J. Wang, Effective mineralization of quinoline and bio-treated coking wastewater by catalytic ozonation using CuFe(2)O(4)/Sepiolite catalyst: efficiency and mechanism, Chemosphere 227 (2019) 647–656, https://doi.org/10.1016/j.chemosphere.2019.04.040.
[61] S.H. Standal, A.M. Blokhus, J. Haavik, A. Skauge, T. Barth, Partition coefficients and interfacial activity for polar components in oil/water model systems, J. Colloid Interface Sci. 212 (1) (1999) 33–41, https://doi.org/10.1006/jcis.1998.5988.
[62] M.T. Carvajal, S. Yalkowsky, Effect of pH and ionic strength on the solubility of quinoline: back-to-basics, AAPS PharmSciTech 20 (3) (2019) 124, https://doi.org/10.1208/s12249-019-1336-9.
[63] M. Huber, M.J. Poller, J. Tochtermann, W. Korth, A. Jess, J. Albert, Revealing the nitrogen reaction pathway for the catalytic oxidative denitrification of fuels, Chem. Commun. 59 (27) (2023) 4079–4082, https://doi.org/10.1039/d3cc00648d.
[64] National Center for Biotechnology Information, PubChem Annotation Record for PYRIDINE, Source: Hazardous Substances Data Bank (HSDB), 2023. Available at https://pubchem.ncbi.nlm.nih.gov/source/hsdb/118. (Accessed November 28th, 2023.
[65] National Center for Biotechnology Information, PubChem Annotation Record for QUINOLINE, Source: Hazardous Substances Data Bank (HSDB), 2023. Available at https://pubchem.ncbi.nlm.nih.gov/source/hsdb/121. (Accessed November 28th, 2023.